Geophysical Signatures of IOCG and Sedex style mineralization in the Mount Isa Eastern Succession, Queensland, Australia

Austin, J.R.[1], Patterson, B.O.[1], le Gras M.[2], Birchall, R.[2],Walshe, J.L.[2]

1. CSIRO Mineral Resources, 11 Julius Ave, North Ryde, NSW, 2113, Australia
2. CSIRO Mineral Resources, 26 Dick Perry Ave, Kensington, WA 6151, Australia

ABSTRACT

The Cloncurry district is renowned for Iron-Oxide Copper-Gold (IOCG) mineralization, but includes a wide spectrum of deposit styles, including: IOCG, Iron Sulfide Copper-Gold, Broken Hill Type (BHT), Sedex, Skarn and intrusion related Cu-Mo. Measurements were made of: density, magnetic susceptibility and Natural Remanent Magnetization (NRM), and Koenigsberger ratios calculated, on 1731 specimens from 14 different mineral deposits and prospects from the Cloncurry district. The deposits studied have a wide variety of petrophysical properties, primarily dictated by the relative contents of magnetic minerals (e.g., magnetite, monoclinic pyrrhotite, and hematite) and other non-magnetic minerals (e.g., hexagonal pyrrhotite, pyrite, galena, sphalerite, barite). Any combination of these minerals can be associated with high densities. High magnetic susceptibilities (and hence high amplitude magnetic anomalies) are invariably associated with coarse magnetite. Monoclinic pyrrhotite is associated with moderate magnetic susceptibility and high remanence, whereas hematite is only weakly magnetic. Many deposits and prospects contain mixtures of different Fe-oxide and sulfide phases, which can be related to redox and/or overprinting. Assemblages usually fall into one of three basic categories: 1.Oxidized assemblages, which contain hematite, no pyrrhotite, but typically pyrite and variable magnetite, are associated with retrograde (magnetite-destructive) alteration, often in association with Cu ± Au- and/or Mo- mineralization. 2. Intermediate assemblages are typically magnetite-rich, but can contain pyrrhotite and/ or pyrite. These are often only weakly mineralized, but are associated with large positive magnetic anomalies, caused by substantial quantities of multidomain magnetite. Magnetite-rich lithologies are advantageous for further mineralization, insomuch as they can be further oxidized or reduced. 3. Reduced assemblages are typically pyrrhotite dominant, contain no hematite, but often do contain magnetite. Hexagonal (non-magnetic) pyrrhotite is typically associated with galena and sphalerite, whereas magnetic pyrrhotite is more typically associated with chalcopyrite. Where monoclinic pyrrhotite is present the remanence is oriented sub-vertical up, and as such, is difficult to isolate from the steep, upward north oriented inducing magnetic field.

INTRODUCTION

The Cloncurry district (the Mount Isa Eastern Succession; Fig 1) is world renowned for Iron-Oxide Copper-Gold (IOCG) mineralization, but in reality the mineralization present is highly diverse, spanning a number of deposit styles, including: IOCG, Iron Sulfide Copper-Gold (ISCG) to Broken Hill Type (BHT), Sedex, Skarn and intrusion related Cu-Mo. Whilst some deposits are monogenetic, many deposits formed via overprinting of two or more different ore forming systems, which occurred during (often interrelated) tectonic, metamorphic magmatic and metasomatic events (Fig 2). The deposits are both mineralogically and petrophysically diverse, and accordingly have wide variability in both their geochemical and geophysical expressions.

This paper presents some of the findings of the Uncover Cloncurry initiative (Austin et al., 2016 a-h). Here we focus on geophysical properties, but the entire report, which includes detailed research on 14 deposits and prospects, plus summary reports for the mineral system is available at: http://bit.ly/2jESB74.

Figure 1: Location map, showing the position of mineral deposits/ prospects studied with RTP magnetics underlain.

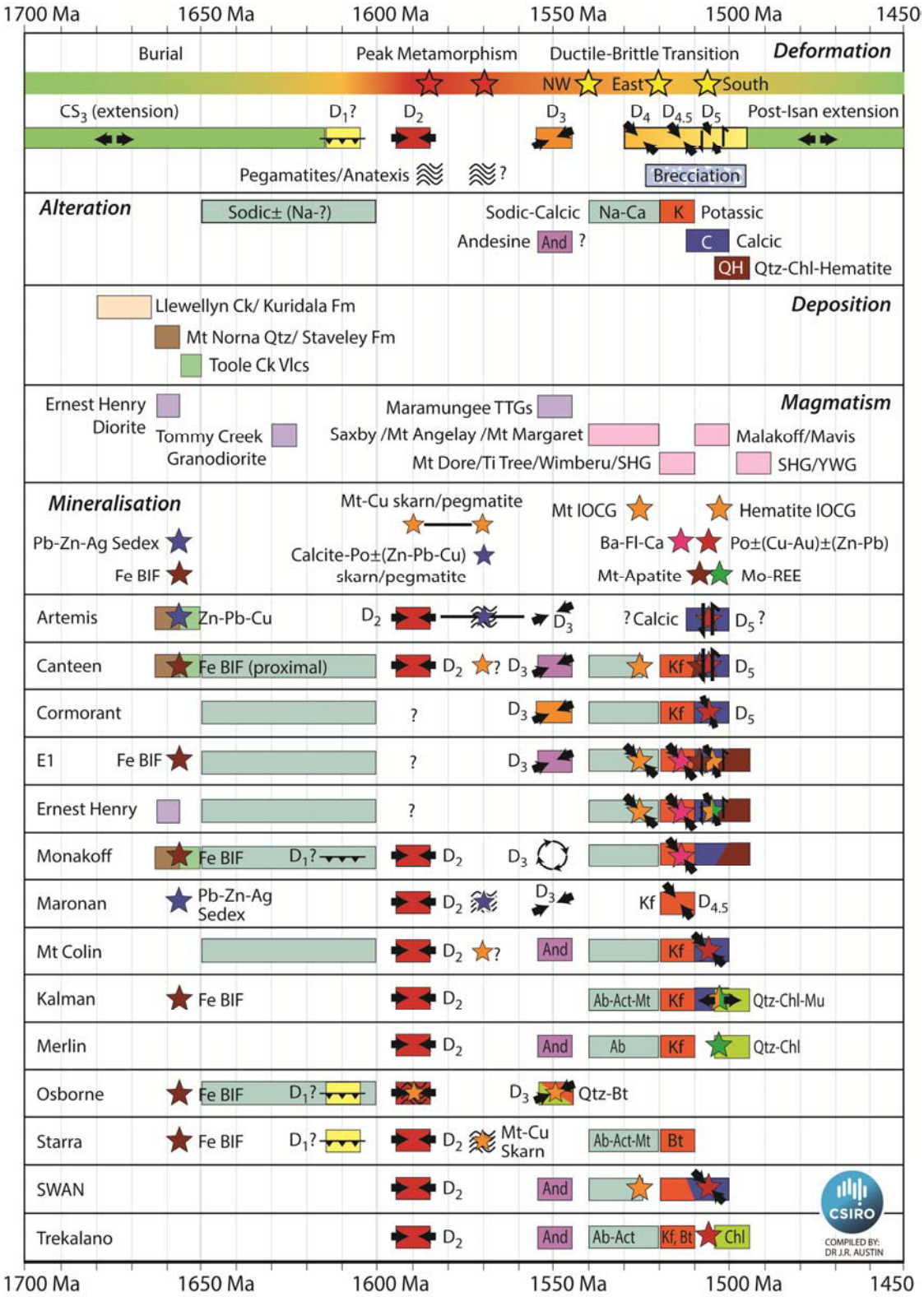

Figure 2: Condensed tectonic, metasomatic and metallogenic history of the Cloncurry District mineral system, and the processes that occurred at each of the deposits and prospects discussed in the study.

PETROPHYSICS OVERVIEW

Measurements of: density, magnetic susceptibility and Natural Remanent Magnetization (NRM) were made on 1731 specimens from 14 different mineral deposits and prospects from the Cloncurry district. The magnetic susceptibility and NRM of each sample were also used to calculate Koenigsberger (Q) ratios, (i.e., the ratio of remanent to induced magnetization).

The petrophysical properties of the ore zones have been assessed by clipping the petrophysical data to the top 10% of measured densities within each deposit or prospect. In general, the top 10% of measurements are correlated with the ore zone for each deposit. However, the extent to which this is true is dependent on the number of samples obtained, and whether those samples accurately reflect the deposit and its host rocks. In cases where the ore zone has been over-sampled the top 10% is likely to be representative. However, where under-sampled the inverse applies. As such, some adjustments were made for individual deposits, to make the results more representative.

The mineralized zones of deposits/prospects assessed by this study have a large range of densities, between 3.1 and 4.8 g/cc (Fig 3). Elevated density can be a result of large concentrations of magnetite, hematite, pyrrhotite, galena, sphalerite, pyrite, and in some cases can be attributed to barite (e.g., at Monakoff; Austin et al., 2016b).

Deposits/prospects have a large range in magnetic susceptibility, from negligible (e.g., 1 x 10^{-6} SI) to 2.1 SI at Osborne (Figs 3, 4). In many cases high densities are correlated with high magnetic susceptibilities (e.g., Fig 3), and in these cases the dominant dense/susceptible mineral is magnetite. For the most part the magnetite is coarse grained, multi-domain magnetite (Fig 4), which does not retain significant, or stable remanence. High densities correlated with low-moderate susceptibilities, are typically due to pyrrhotite. High densities and negligible susceptibilities can be related to hematite, pyrite, hexagonal pyrrhotite, and/or practically any species of sulfide.

The various deposits have a range of natural remanent magnetization (NRM) intensities, from negligible up to mean values of 450 A/m, and associated Koenigsberger ratios of up to 130 (Fig 4). Prospects which have high Koenigsberger ratios (e.g., Cormorant, Canteen) contain monoclinic pyrrhotite as the dominant magnetic phase.

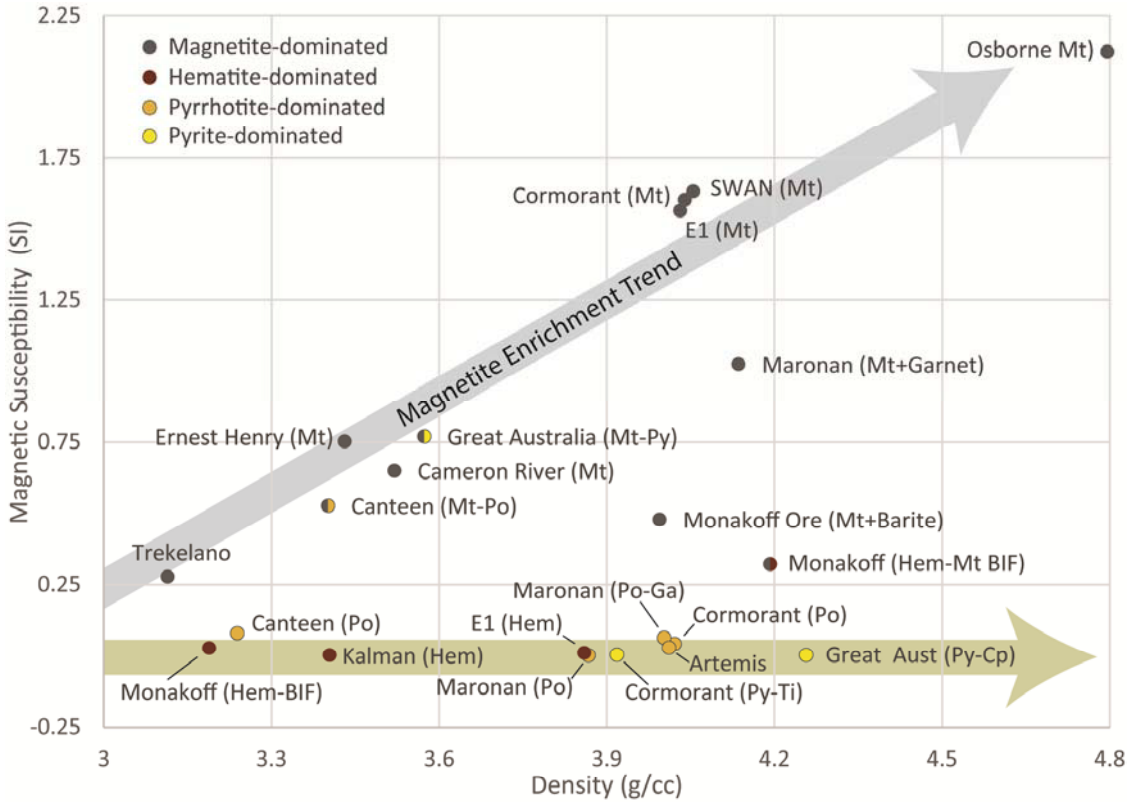

Figure 3: Plot of magnetic susceptibility vs density for ore samples from deposits / prospects assessed in this study.

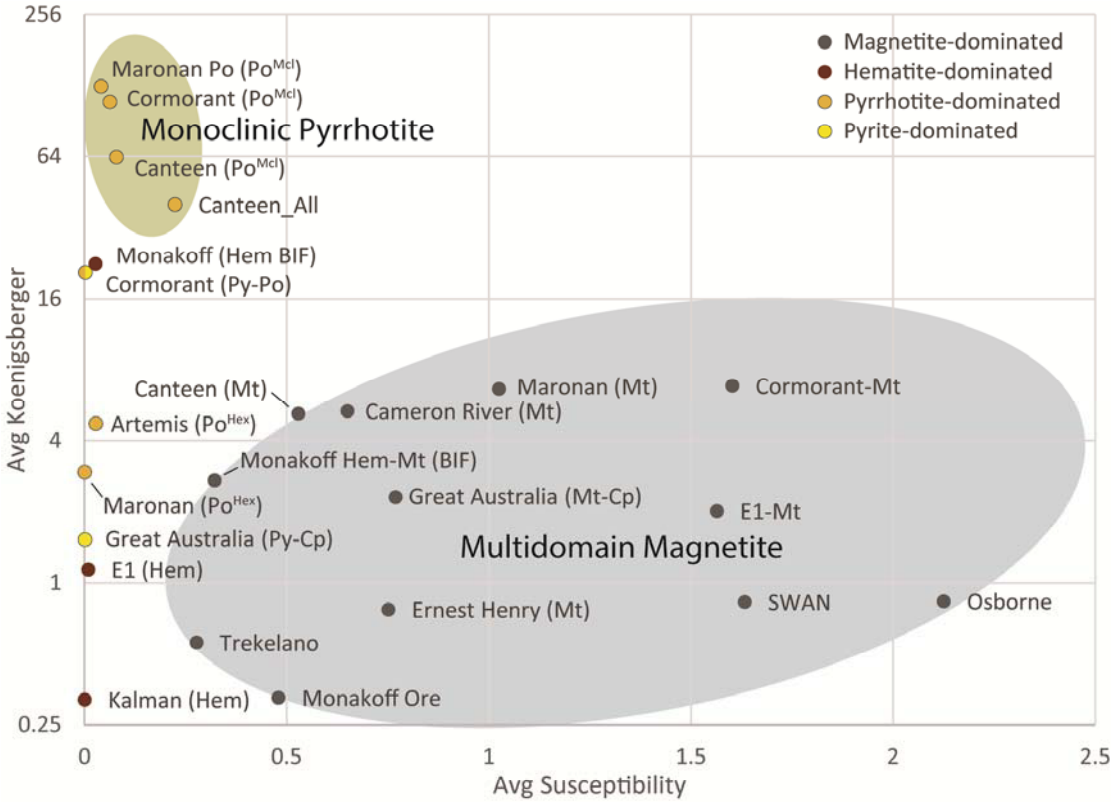

Figure 4: Plot of the ratio of NRM to magnetic susceptibility (Q, Koenigsberger Ratio) vs magnetic susceptibility for ore samples from deposits / prospects assessed this study.

In terms of petrophysical properties there are several recognized associations:

1. Deposits with high density, high susceptibility, and low Q ratios are dominated by coarse MD magnetite, e.g., Osborne, SWAN.
2. Deposits with high density, high susceptibility and moderate Q ratios (e.g., Cormorant, Maronan) may contain pseudo single domain (PSD) magnetite which may be indicative of a sedimentary origin.
3. Deposits with high density, low susceptibility, and high Q are rich in monoclinic pyrrhotite, e.g., Cormorant, Canteen.
4. Horizons with high density, low susceptibility, and moderate Q may be indicative of metamorphosed hematite, e.g., Monakoff West BIF.
5. Deposits with high density low susceptibility, and low Q may contain hexagonal pyrrhotite and /or sphalerite, galena, pyrite and hematite, i.e., are associated with a relative absence of magnetite.

Many specimens contain mixtures of different Fe-oxide and sulfide phases. These different assemblages may be related to redox gradients and /or overprinting by different metasomatic events. However, the assemblages usually fall into one of three basic categories, with some overlap.

1. Oxidized assemblages contain hematite, and do not contain pyrrhotite, but typically are associated with pyrite ± chalcopyrite, and typically contain minimal amounts of magnetite.
2. Intermediate assemblages are typically magnetite-rich, and may contain pyrrhotite and /or pyrite, but typically only in small proportions. Many magnetite-rich lithologies are often also apatite-rich.
3. Reduced assemblages are typically pyrrhotite dominant, contain no hematite, but often do contain magnetite. In these cases, hexagonal (non-magnetic) pyrrhotite is typically associated with galena and sphalerite. Monoclinic (magnetic) pyrrhotite is more typically associated with Cu prospects, however this is only a qualitative observation.

The relationships between oxidation state and magnetic expression are illustrated in Fig 5.

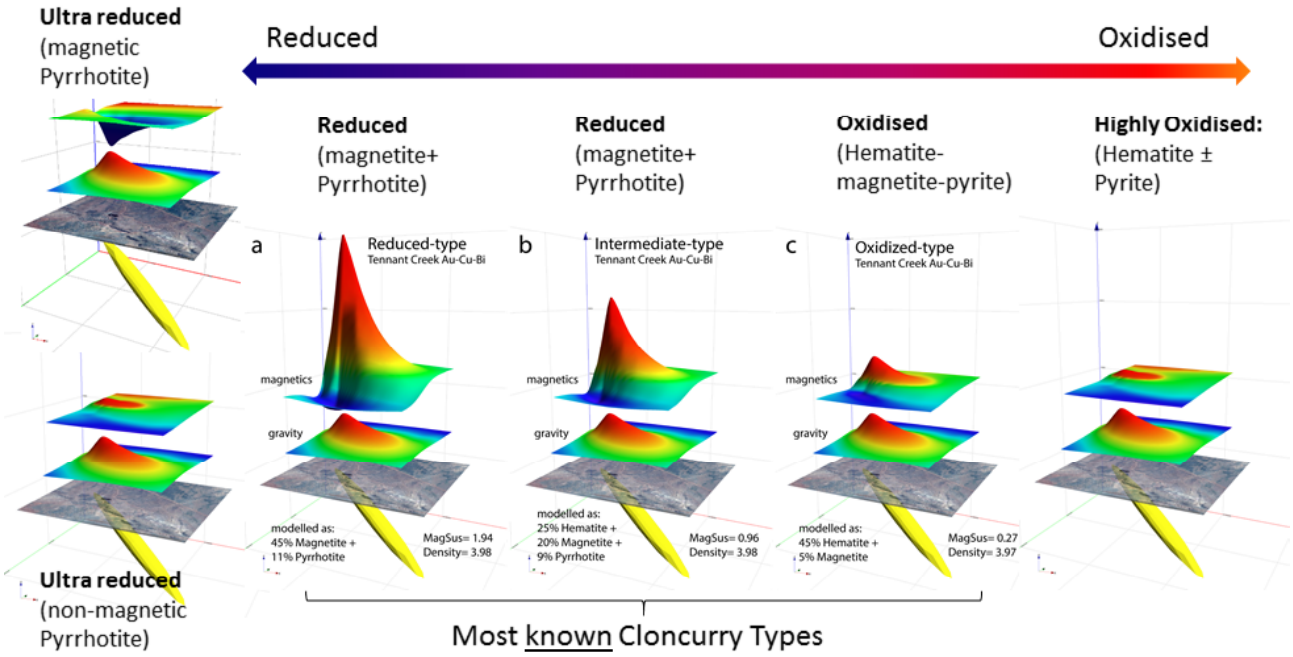

Figure 5: Synthetic models of the El Dorado deposit, Tennant Creek (based on Austin and Foss, 2014), which contain different proportions of Fe-oxide and Fe-sulfide minerals, based on their Redox state. All the mineral assemblages have comparable density, but the different redox states have very different geophysical expressions.

SYN-DEPOSITIONAL SEDEX/BHT & DISTAL BIF MINERALIZATION AT *ca* 1650 MA

The early BHT/ Sedex-style Pb-Zn-Ag mineralization and the associated barren distal BIFs have a similar geophysical expression. In both cases the mineralization is stratiform, and therefore associated with bedding parallel elongate magnetic anomalism. In general, BHT/ Sedex and the corresponding distal BIFs contain significant magnetite. However, there appears to be a redox control on the species of Fe-oxide, whereby mineralization closer to the source is more reduced (e.g., magnetite ± pyrrhotite) whereas the more distal deposits are more oxidized (e.g., hematite ± magnetite). In general this is coupled with corresponding zonation of metals, with greater economic minerals closer to the core of the system, and greater sediment content distal to the vent.

In terms of geophysical response, the distal parts of these systems generally have fairly consistent, stratiform, laterally extensive, but low amplitude magnetic anomalies, associated with relatively modest magnetic susceptibility (e.g., the anomalies that sit close to the contact between the Mt Norna Quartzite and the Toole Creek Volcanics in the Pumpkin Gully Syncline; near Monakoff; Austin et al., 2016b). Measured samples from this horizon show significant variability in their petrophysical properties, related to both oxidation state and total Fe- oxide content. The distal BIF near Monakoff is hematite-rich along strike to the west where it has a mean susceptibility of ~0.03 SI, a Q ratio of ~13, and a density of ~3.2 g/cc. Conversely, along strike to the east, the BIF contains both hematite and magnetite, with a mean susceptibility of ~0.3 SI, a Q ratio of 1.5, and a density of 4.2 g/cc (see Figs 6, 14, 15). In this case the eastern BIF has a total magnetization approximately twice that of the hematite BIF. However, the total remanence is only 33% greater in the east BIF, and the relative remanence (the Q ratio) of the hematite-rich BIF is much higher.

Parts of a Sedex system that are proximal to the vent commonly sit along-strike of these subtle stratiform anomalies, but they coincide with much higher amplitude anomalies, which are a result of thicker magnetized horizons and/ or greater magnetite content, e.g., Osborne and Maronan (Gazley et al., 2016b; Austin et al. 2016c). The vent-proximal mineralization at Maronan for example has a mean susceptibility of ~0.6 SI and a Q ratio of ~5.3 and a density of ~3.7 g/cc. (Fig 7) In this case the proximal BHT/Sedex-style mineralization has a total magnetization approximately 25 times that of the hematite BIF, and 7 times greater than the magnetite-hematite BIF at Monakoff. However the main mineralized zone which sits in-between the magnetic anomalies has a completely different pyrrhotite-rich mineralogy (discussed shortly).

The deposits at both the Pb-Zn and Cu-Au end-members of this system are overprinted in a number of different ways during subsequent metamorphism, deformation and metasomatism, and these processes can potentially lead to enhancement of the magnetic signal (addition of magnetite/pyrrhotite), destruction/depletion of the magnetic signal (i.e., magnetite destruction; including removal of Fe, oxidation of magnetite to hematite, reduction of magnetite to pyrrhotite), or modification of the magnetic signal from a largely induced magnetization (i.e., held in multi-domain (MD) magnetite) to a largely remanent magnetic signal (i.e., held in monoclinic pyrrhotite). Several of these scenarios are discussed further in following sections.

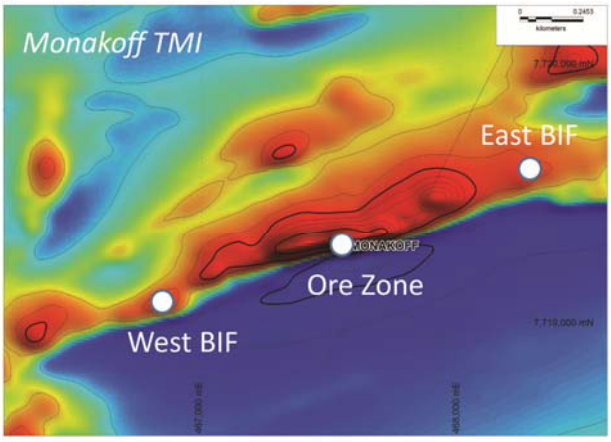

Monakoff	Density (g/cm^3)	Mag Sus K (SI)	Koenigsberger Ratio (Q)
host rocks	2.81	0.0014	-
BIF West (Qtz-Hem)	3.19	0.03	12.27
BIF East (Qtz-Mt-Hem)	4.19	0.32	1.54
Ore (Mt-Cp-Py)	3.99	0.48	0.16

Figure 6: Comparison of the geophysical signatures and petrophysical properties associated with the Monakoff deposit and Maronan prospect, both of which are interpreted to have initially formed as BHT/ Sedex systems.

PEAK METAMORPHIC PYRRHOTITE "SKARNS" AT *ca* 1590 - 1570 Ma

Calcite-rich assemblages that are totally recrystallized, or newly precipitated are often referred to as "skarns" across the Cloncurry district (as discussed in Austin et al., 2016a). If these are skarns, they are not typical skarns, formed via interaction of magmatic fluids with carbonate rocks. However, they may be reaction skarns, i.e., formed via chemical interaction of adjacent protoliths. For example adjacent BIF and calcsilicate rocks at Starra may form a magnetite-dolomite-chalcopyrite reaction skarn during peak metamorphism. In other cases, e.g., Maronan, the coarse-grained calcite-pyrrhotite-galena assemblage sits in the core of the BHT/ Sedex system, and is potentially just a recrystallized version of the protolith. In terms of their geophysical response, the two types of peak-metamorphic assemblages discussed below have a very different response. However, in each case the properties may not differ substantially from the protolith(s).

Pyrrhotite ± Pb-Zn-Cu melts (skarn)

Pyrrhotite ± Pb-Zn-Cu "skarn" occurs at Artemis, Altia and Maronan. At Maronan the "skarn" is located in the central part of the mineralized zone, with magnetite-dominated lithologies occurring to the north and south along strike. This is consistent with the Sedex mineralization model whereby there is a zonation within the deposit, from reduced assemblages (e.g., pyrrhotite – rich; Fig 8, below) in the core, to moderately oxidized assemblages proximally (e.g., magnetite; Fig 8, top) and more oxidized distally (e.g., hematite).

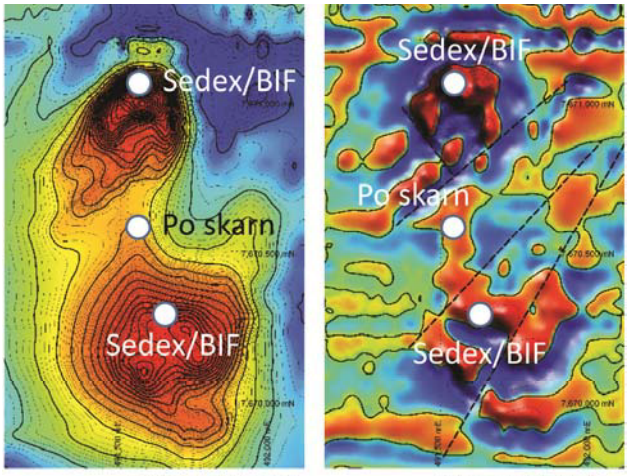

Maronan	Density (g/cm^3)	Mag Sus K (SI)	Koenigsberger Ratio (Q)
host rock	2.91	0.01	11.37
Po skarn	3.27	0.01	62.17
Potassic Alt	2.91	0.37	0.99
Sedex	3.71	0.62	5.32

Figure 7: Comparison of the geophysical signature and petrophysical properties associated Maronan prospect. Note the relatively subtle magnetic signature of the core of the anomaly, labelled "Po skarn".

Whilst these assemblages are sometimes referred to as "skarns", it is not necessary that the mineralogy is changed substantially in the core of the system during the formation, e.g., a calcite–pyrrhotite mineralogy may be common to both. However, we infer that the pyrrhotite within the system can change its crystal structure, from monoclinic to hexagonal pyrrhotite as a result of recrystallization during metamorphism. At Artemis (Fig 9) pyrrhotite appears to be almost entirely hexagonal (non-magnetic) within the mineralized core of the system. More distal to the mineralized zone, there are magnetic rocks (inferred from modelling), particularly to the north and above, which sit at the fault intersection. This suggests redox zonation within the mineral system, possibly related to near surface oxidation.

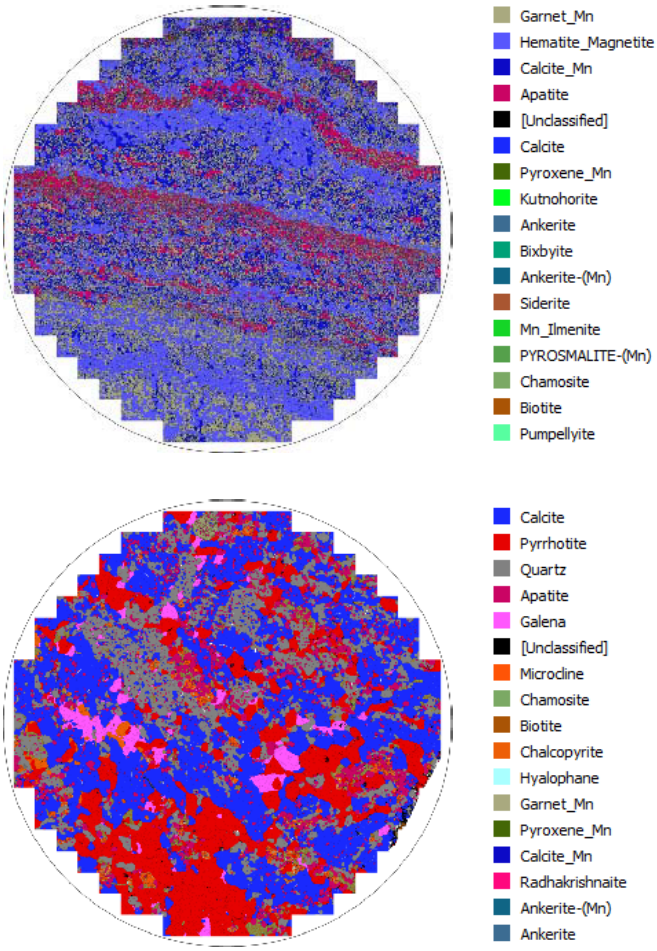

Figure 8: TIMA (Tescan integrated mineral analyzer) imagery of: Top. Banded garnet-magnetite-calcite sample from the distal 'Sedex" part of Maronan, and; Below. Relatively reduced pyrrhotite-galena-calcite rock with an equigranular (recrystallized) texture, from the core of the system. All TIMA scans are approx. 22mm in diameter.

By contrast, at Maronan, monoclinic (magnetic) and hexagonal (non-magnetic) pyrrhotite are both clearly present within the mineralized Po-"skarn" assemblages. Where there is monoclinic (magnetic) pyrrhotite, remanence is very strong and the remanence directions are typically sub-vertical and upward oriented. This suggests that they should form relatively symmetrical positive magnetic anomalies for upright bodies (i.e., bodies with no significant dip). Similar calcite-pyrrhotite mineralogies are also encountered at Canteen, and these also have sub-vertical upward oriented magnetizations, but are not associated with mineralization.

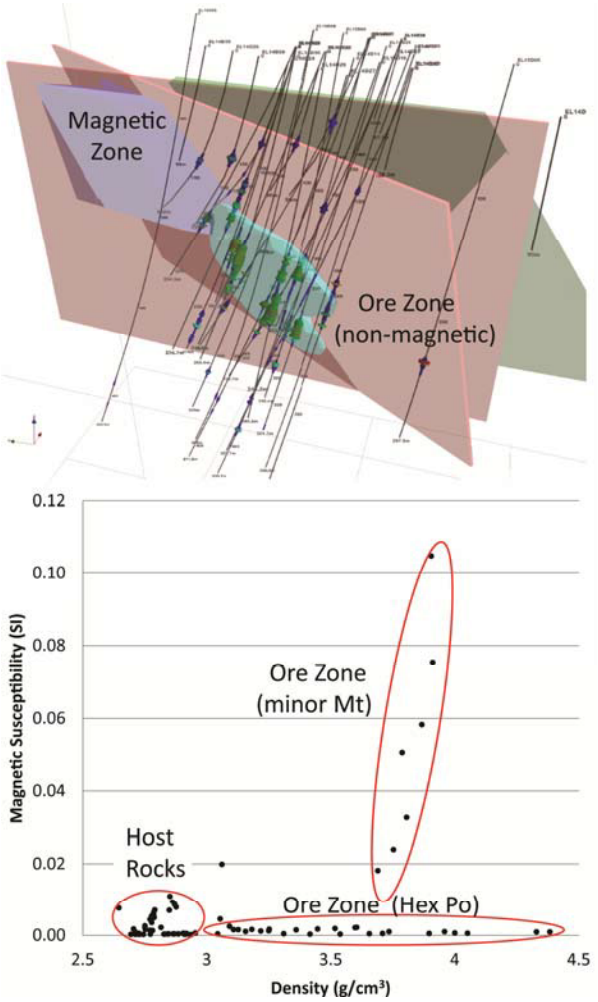

Figure 9: Density vs magnetic susceptibility plot for Artemis (lower) indicates that the sulfides present within the ore zone are generally non-magnetic. The ore zone at Artemis (in turquoise; above) is primarily associated with hexagonal (non-magnetic) pyrrhotite. However, more distal to the mineralized zone, there is a zone of high susceptibility (deduced by magnetic modelling) at the fault intersection (purple).

Magnetite ± Cu skarn

Magnetite ± Cu "skarn" is observed at Starra, and may also be present at Osborne. At Osborne, we do not have enough data to differentiate the peak-metamorphic mineralization from the earlier sedex/BIF mineralization. However, at Starra, the dolomite-magnetite±chalcopyrite assemblages are distinct from other "ironstones" and "BIFs" regionally, which tend to be associated with quartz, apatite and sometimes feldspars (e.g., at Osborne) rather than carbonate.

Dolomite-magnetite±chalcopyrite assemblages at Starra are strongly Magnetized, with mean susceptibility of ~1.63 SI and a Q ratio of ~0.8 and a density of ~4.06 g/cc. BIF/sedex style mineralization at Osborne has a mean susceptibility of ~1.77 SI and a Q ratio of 0.9 and a density of ~4.29 g/cc. The measured Q is likely to be approximately 3times greater than the *in situ* Q due to drilling induced magnetization. Hence the real Q is probably closer to 0.3, which means that remanence is not a significant contribution to the magnetic field expression of the deposit. The geophysical properties are almost identical to those at Osborne, which might be due to their common genesis as skarn mineralization derived from a BIF/sedex protolith. The main contrast is that the "skarn" at Starra has a lower density, owing to the greater proportions of dolomite compared to silicate minerals (which are denser), and distinct lack of apatite.

POST-METAMORPHIC, PRO-GRADE HYDROTHERMAL SYSTEMS (*ca*1530 - 1515 Ma)

The main types of alteration which appear to be synchronous with D_4 (*ca* 1530-1525 Ma) are magnetite-apatite alteration, observed at Ernest Henry at Canteen and at E1 and the sodic (±calcic) alteration observed in numerous deposits across the district.

Magnetite-Apatite-dominated systems

Magnetite-apatite assemblages, e.g., Fig 10 (top), are common in IOCG-style deposits, particularly the Kiruna-type sub-class (e.g., Nystroem and Henriquez, 1994). Such alteration, is associated with extreme susceptibility, large magnetic anomalies (e.g., Fig 11) but relatively minor, (viscous) remanence, which together are typical of multidomain magnetite. Sample EHM005 from Ernest Henry had a magnetic susceptibility of ~1.8 SI and a Q ratio of ~0.5 (NB: remanence is likely amplified by ~300% due to drilling induced magnetism (DIM), so the *in situ* Q would be 0.1-0.2). Similar samples drilled from the pit at E1 (e.g., samples E1-K and E1-M) also have mean magnetic susceptibilities ranging from 1.5 – 2.0 SI, and Koenigsberger ratios of 0.1 – 0.2. (NB: because these were surface sampled, they are not affected by DIM).

Although the radiometric signatures of different alteration types are not well understood, there is a correlation between U-rich radiometric signatures (e.g., Fig 12) and the highly magnetic zone at Canteen as indicated by the shading in Fig 12. The U-rich signature at Canteen is correlated with magnetite-apatite alteration within that system, and potentially at other deposits and prospects within the district. However, U-rich radiometric signatures are also correlated with sodic alteration at redox boundaries (e.g., Cormorant, Fig 16). We therefore infer that the two alteration types are related.

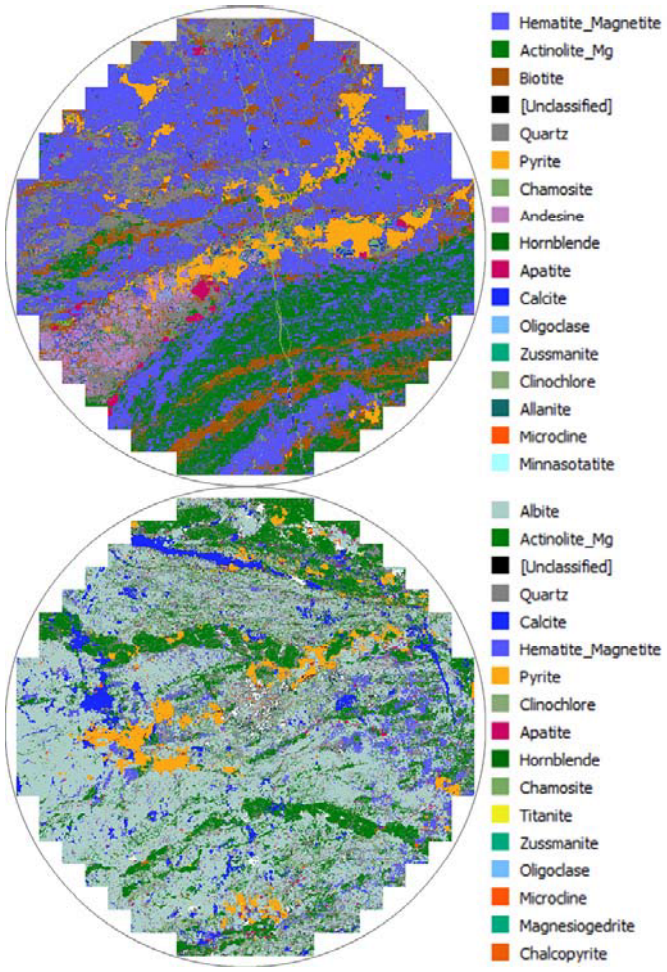

Figure 10: Examples of magnetite-apatite assemblages (sample CAN034) and sodic-calcic alteration (albite-actinolite-magnetite; sample CAN016) observed in TIMA data from Canteen prospect.

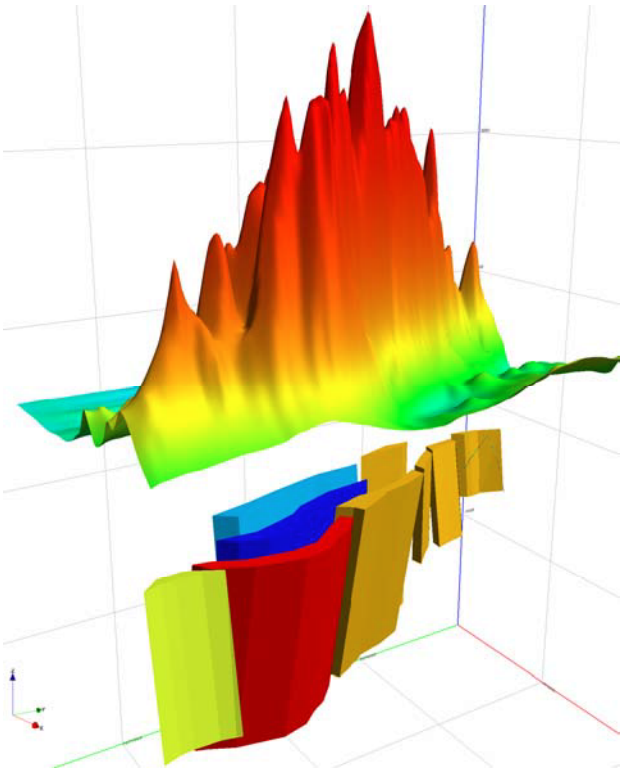

Figure 11: 3-D perspective view of the modelled bodies, with a rendered version of the TMI field above. NB. The TMI anomaly is zoned, with the highest intensity toward the center of the magnetized zone.

Sodic Alteration (albite-magnetite-titanite)

Sodic alteration tends to be mainly manifested by albite-dominated lithologies with variable amounts of magnetite as the main magnetic phase. It can be pervasive, particularly within calc-silicate dominated units, e.g., the Doherty and Corella formations. It has similar petrophysical properties to the magnetite-apatite alteration (already discussed), sits along the same susceptibility – density trend (e.g., Fig 17) and is possibly genetically related. However, sodic alteration is less magnetic, due to its lower magnetite content (as shown in Fig 10, lower). The proportion of magnetite (and titanite) within sodic altered lithologies is variable, but significantly less than for magnetite-apatite altered rocks. For example, the mean susceptibility of sodic altered samples from Ernest Henry is 0.76 SI, which is high, but approximately 50% of the susceptibility of magnetite-apatite altered samples from Ernest Henry and E1. The sodic alteration also has relatively minor remanence, with Q ratios of ~0.1 to 0.2 (after a DIM correction is applied). Therefore, the magnetic expression of sodic alteration is variable, but is commonly associated with moderate to high susceptibility and low remanence, which is typical of moderate amounts of coarse multi-domain magnetite.

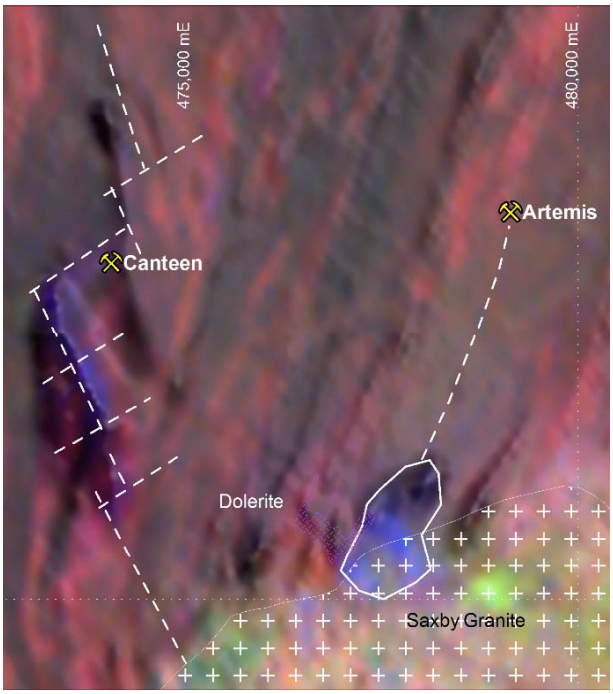

Figure 12: Ternary radiometric image for the Canteen and Artemis area in which: red = K; green = Th; and blue = U. RTP magnetic overlain as shading. (Austin et al., 2016e).

Potassic Alteration

Potassic alteration is present throughout the Cloncurry district, but tends to be less pervasive than sodic alteration. Potassic alteration can take two main forms; replacement of sodic and/or calcic feldspars by K-feldspar, e.g. Fig 13 (top), and/or replacement of ferromagnesian minerals by biotite, e.g. Fig 13 (lower). Potassic alteration is typically considered to be associated with hematite (based on the reddish color of the K-feldspar). However, magnetite is the dominant magnetic phase in K-feldspar altered mineralized lithologies, assessed in this study.

Potassic alteration is associated with mineralization at a number of deposits and is also present within non-mineralized zones of other deposits and prospects, e.g., Maronan (Austin et al., 2016c) where it is localized by a number of cross-cutting faults in the core of the system. It can be both magnetite and pyrrhotite-destructive, e.g., via oxidation (formation of hematite ± pyrite) and/or uptake of Fe into biotite. However, it is usually coincident with at least some magnetite within mineralized systems. It is associated with molybdenum at Merlin but predates mineralization (Patterson et al., 2016). At Osborne, Cu mineralization is associated with retrograde biotite (Gazley et al., 2016b) and at Ernest Henry, K-feldspar alteration is associated with relatively moderate levels of chalcopyrite mineralization (Austin et al., 2016d).

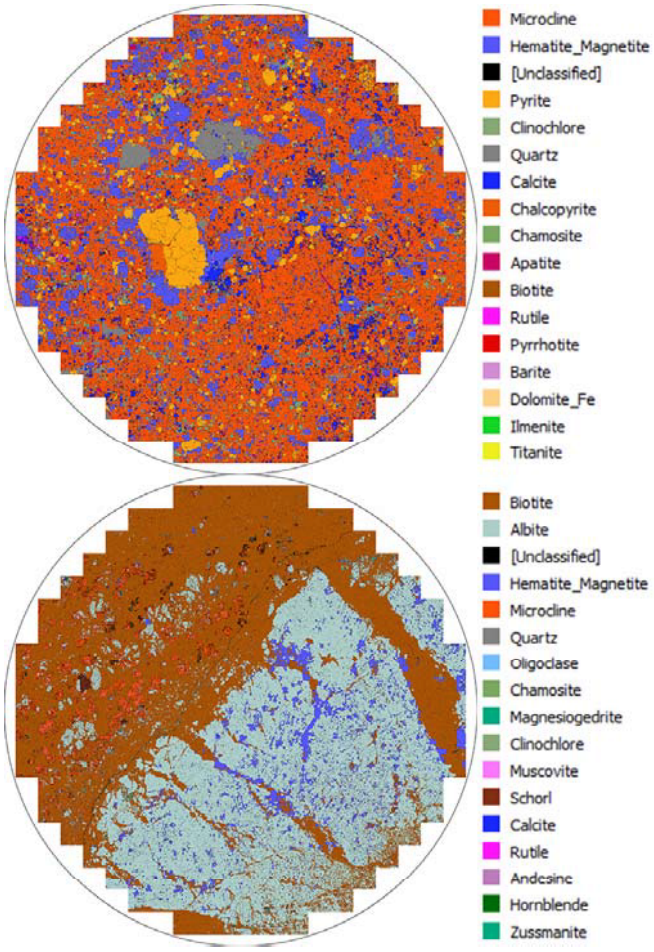

Figure 13: Some typical potassic alteration from Ernest Henry. Top. Pervasively altered mineralogy comprised of K-feldspar, magnetite/hematite, and pyrite in sample EHM025. Below. Biotite-K-feldspar partially overprinting sodic alteration (albite-magnetite) in sample EHM004.

Assessment of the petrophysical properties of rocks from Ernest Henry suggest that where sodic alteration is overprinted by potassic (K-feldspar) alteration, the magnetic susceptibility is reduced by 30 – 50% compared to the sodic altered rocks (e.g., Fig 21). Some of this reduction could be attributed to oxidation of magnetite to hematite. However, the potassic altered rocks do generally still sit on the same susceptibility/density trend as magnetite-rich rocks, suggesting they do not contain significant hematite. Some iron may have formed pyrite, but again the formation of pyrite cannot be significant for the aforementioned reason. It seems most likely that the majority of Fe produced from the destruction of magnetite is going into biotite and potentially chlorite (chamosite) during potassic alteration.

Magnetite-barite-fluorite-calcite alteration

Magnetite-fluorite-barite-calcite alteration assemblages are present within Monakoff, E1 and to a lesser extent Ernest Henry (Austin et al., 2016b, e, d). Monakoff provides the best example, in which there is clear zonation between the host BIF discussed previously and the magnetite-fluorite-barite-calcite-chalcopyrite zone that overprints it. The main high susceptibility lithologies, and by association, the sources of the magnetic anomaly at Monakoff, include a magnetite BIF and the magnetite-barite-fluorite-rich mineralized zone (Fig 14, upper). Both have mean susceptibilities of ~0.5 SI and both units share a linear susceptibility/density gradient, as shown in Figure 14 (lower).

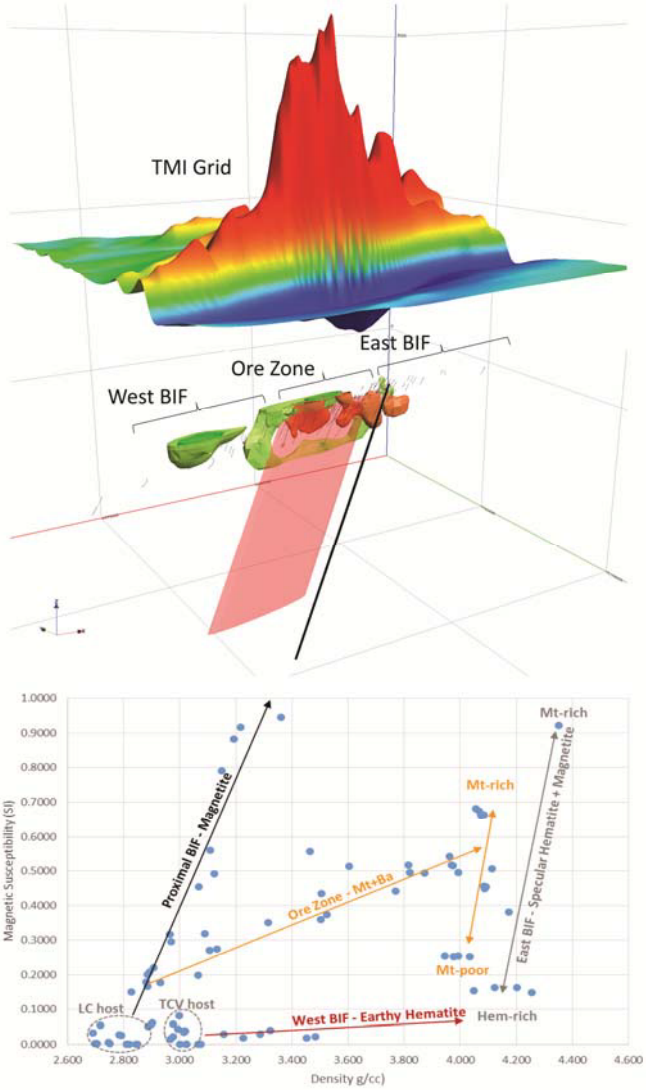

Figure 14: Plot of magnetic susceptibility vs density for samples from the Monakoff mine. The different trends correspond to different mineralization styles.

The magnetite BIF tends to be high susceptibility with lower density, and this is due to magnetite being the main magnetic phase and high SG mineral (SG_{Mt} = 5.15 g/cc). Conversely, the mineralized horizon tends to have much higher, which is in part due to iron being taken up in Fe-sulfides (SG_{Py} = 5.02 g/cc), but mostly due to the high volume of barite (SG_{Ba} = 4.5 g/cc) present within the mineralized assemblage. Within the mineralized zone there are a range of susceptibilities which occur within a broadly comparable density range, and hence there is significant variability in the magnetite content. The magnetite-fluorite-barite-calcite-chalcopyrite overprint has very similar magnetic properties to the magnetite-BIF protolith, but is distinguished by its strong NE-oriented fabric, which crosscuts the E-W layering of the host BIF. Austin et al. (2016b) demonstrated that the magnetite-fluorite-barite-calcite-chalcopyrite overprinted the BIF, and that the redox zonation from relatively oxidized to more reduced (intermediate) assemblages were associated, to some extent, with overprinting. However, as discussed previously in relation to Maronan, it is quite possible that the mineralized zone formed within a Sedex horizon and was already barite- and magnetite-rich. So it is possible that this alteration style is really a pre-existing mineralized zone that was recrystallized via metasomatism at *ca* 1515 Ma.

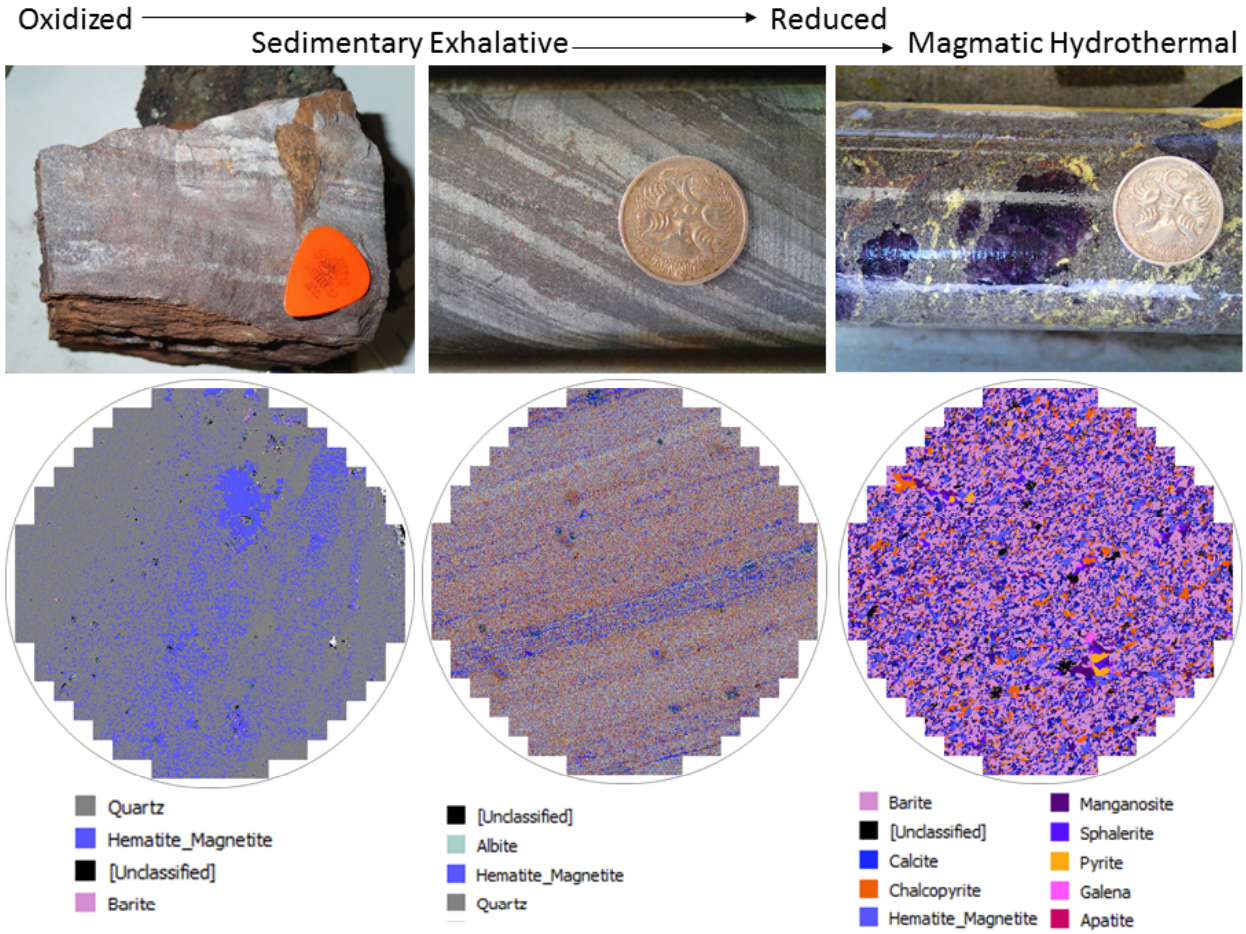

Figure 15: Transition from highly oxidized (Left) to relatively reduced assemblages (middle) within an early Sedex system at Monakoff. The system was overprinted by a magmatic fluid leading to a Cu-, Barite and Fluorite-rich recrystallized ore.

PYRRHOTITE ASSEMBLAGES

Calcite in association with coarse pyrrhotite is present at a number of other prospects and deposits (e.g., Canteen, Maronan, and Artemis; Austin et al., 2016 b, e, f). However, it is not clear that they are co-genetic. In all cases, the textures are relatively undeformed. However, some assemblages appear to have formed in zones of dilation, e.g., veins and breccia matrix, others appear to have formed by recrystallization. The former are consistent with late brittle deformation, whereas the latter are more consistent with high temperature metamorphic conditions, e.g., Artemis, Maronan, discussed previously.

Canteen

At Canteen the alteration paragenesis is fairly complex, due to the variable origin of the protoliths, with some clearly mafic igneous in origin and others sedimentary (Austin et al., 2016e), leading to commensurate variations in altered mineralogy. The early phase of alteration consists of albite and/or andesine, in association with actinolite, (fine) magnetite, apatite, titanite and pyrite. This is variably overprinted by patchy potassic alteration, which is either K-feldspar-, or biotite-rich, depending on the protolith. The calcite-pyrrhotite phase is associated with both quartz and dolomite at Canteen and is observed as veining and breccia infill (Fig 16).

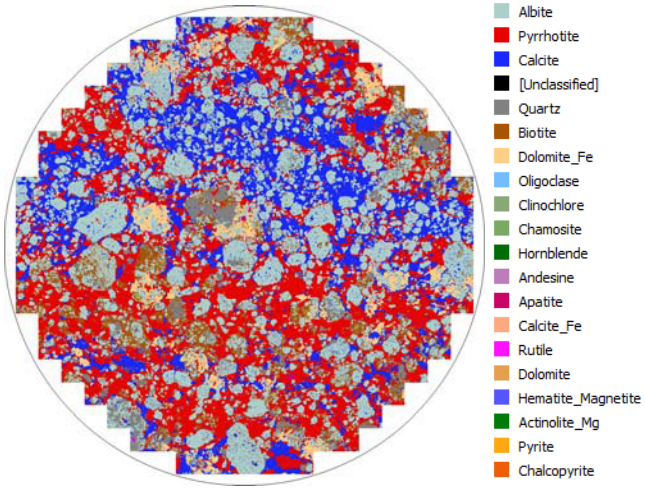

Figure 16: TIMA imagery from Canteen which show the calcite-pyrrhotite assemblage overprinting albitized rocks at Canteen, as a breccia matrix.

However, the morphology of the veining suggests that the veins are actually a proto-breccia texture. Both clearly overprint several earlier alteration phases, most notably: pervasive sodic (albite) alteration; a magnetite-pyrite-apatite assemblage (which appears to be common to several other deposits); and potassic alteration. Although the mineralogy is similar to that observed at Artemis and Maronan (Austin et al., 2016 f, b), the textural context of the calcite-pyrrhotite phase suggests that it is a relatively late alteration phase.

Cormorant

At Cormorant textural evidence suggests that the mineralization is associated with pyrrhotite in a series of microbreccias and veins (Fig 17, 18; Austin et al., 2016c). Cormorant is distinct from most of the other pyrrhotite-rich deposits/prospects (e.g., Canteen and Maronan) in that the pyrrhotite is not associated with calcite. In many cases albite-pyrrhotite-chalcopyrite and titanite are intergrown (Fig 17), but in other samples the titanite, chalcopyrite and pyrrhotite occupy cracks and grain boundaries in massive albite. Mineralization is associated with pyrrhotite-dominant vein phases (Fig 18), and it appears that the fluid responsible for alteration is reduced since it precipitated large volumes of pyrrhotite but small amounts of chalcopyrite. Elevated Cu occurs either side of an apparent redox boundary at approximately 450 m in the studied drill-hole (Fig 19). Here we see a transition down hole from magnetite dominant (400–425 m) into magnetite-pyrrhotite (425–450 m) into pyrrhotite dominant (450–500 m), and then titanite dominant lithologies (500–550 m).

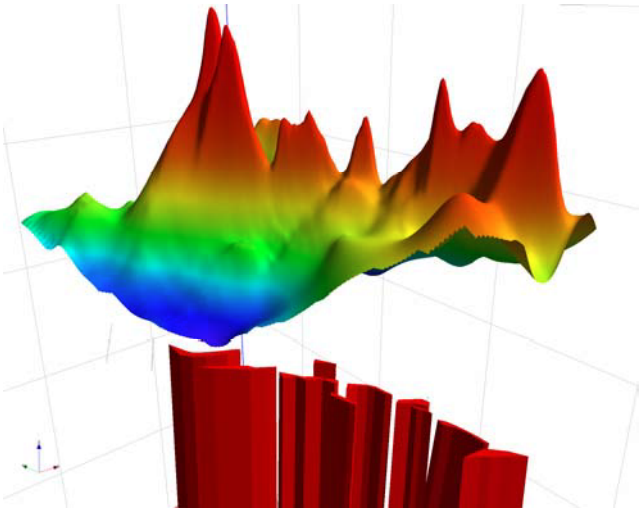

Figure 17: Perspective view of the Cormorant magnetic model, in relation to a 3-D rendering of the magnetic field. Viewed toward the NE. The graticule spacing is 1km.

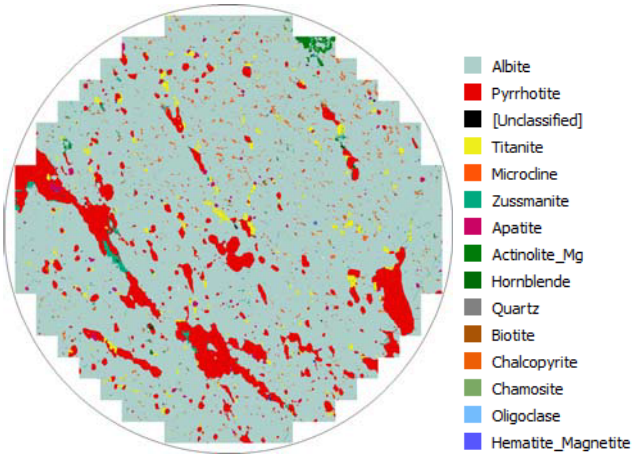

Figure 18: Two Albite-pyrrhotite-chalcopyrite-titanite assemblages from Cormorant (COR015).

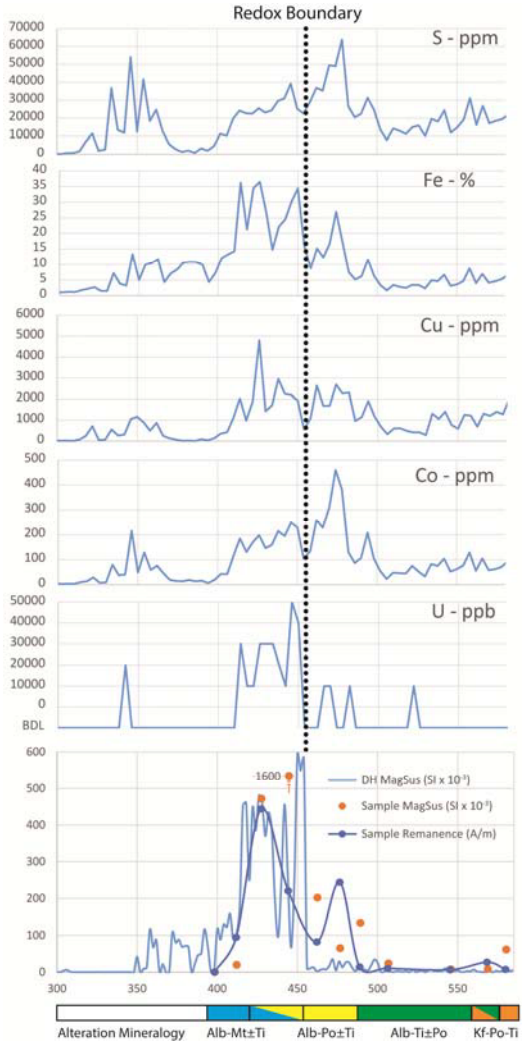

Figure 19: Comparison of assay data with down-hole susceptibility, measured susceptibility and remanence.

Remanence in Monoclinic Pyrrhotite

Monoclinic pyrrhotite in several of these deposits (e.g., Canteen, Cormorant, Maronan, Mt Colin) is associated with high Koenigsberger ratios. However, the associated remanence directions are generally very similar, with sub-vertical upward oriented magnetizations. Such magnetizations are consistent with metamorphic resetting associated with intrusion of voluminous mafic magmas at *ca* 1114 Ma, (Austin et al. 2016 b, f, g, h). The magnetizations are sub-vertical and sit within a N-S plane in a similar orientation to the inducing Field. Hence, although pyrrhotite-dominated mineralization has a characteristic remanent magnetization, it is not different enough to the inducing field to allow remote mapping, and therefore is not effective as an exploration tool.

POST METAMORPHIC RETROGRADE ALTERATION AT *ca* 1510-1500 Ma

Quartz-calcite-chlorite-hematite alteration

Late quartz-calcite-chlorite-pyrite-hematite alteration is present in a number of deposits and prospects in the Cloncurry district, and is associated with copper and/ or molybdenum mineralization at Ernest Henry, Canteen, Kalman and Merlin (Austin et al., 2016 d, f; Gazley et al., 2016 b; Patterson et al., 2016). This alteration is the most oxidized style observed in the Cloncurry district, as indicated by the presence of pyrite and hematite, rather than pyrrhotite and magnetite (Fig 20). This is further demonstrated by Fig 21, in which mineralized samples (with such alteration) sit below the magnetite trend on the density/susceptibility plot. This suggests that the iron in magnetite is not only being converted to ferromagnesian minerals (e.g., chamosite), but also chalcopyrite, pyrite and/or hematite during the late alteration history. Therefore, these samples are oxidized relative to the system as a whole, which is magnetite dominant.

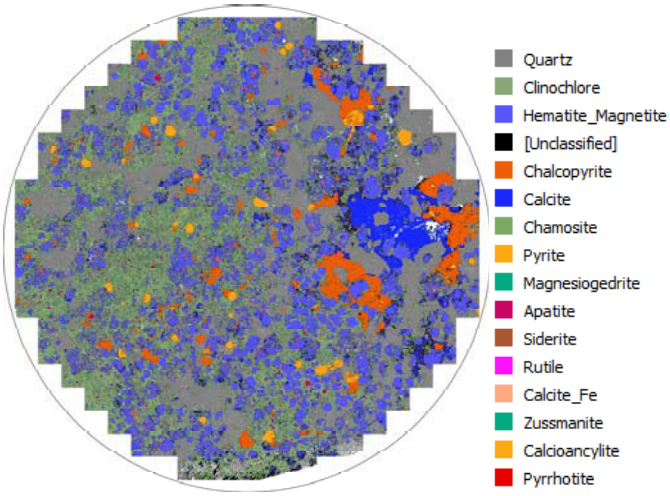

Figure 20: Typical Quartz-hematite-chlorite-chalcopyrite assemblage from the Ernest Henry ore zone.

Ernest Henry

A comparison of the different alteration types at Ernest Henry was compiled based on key mineralogies within the deposit (Table 1). The results reveal that sodic alteration has no association with Cu-mineralization, and that potassic alteration has only a minor spatial association with mineralization as mentioned previously. However, quartz-calcite-chlorite alteration has a major spatial association with Cu mineralization (Table 1). So for Ernest Henry there is an inverse redox gradient. The most oxidized parts of the system contain the majority of Cu mineralization, whereas the more reduced parts

generally do not. Geophysically, the mineralized zone is less magnetic than the enveloping potassic alteration, which in turn is significantly less magnetic than the enveloping sodic alteration (Fig 22). This complexity of overlapping zones and cumulative magnetization contrasts is why the ore-pipe at Ernest Henry is so difficult to model (e.g., Austin et al. 2016d).

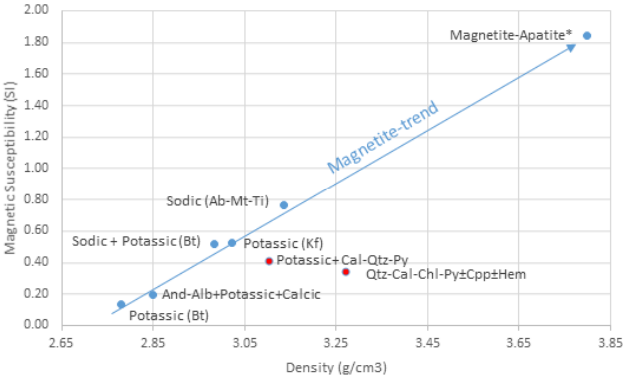

Alteration	Density (g/cm^3)	Mag Sus K (SI)	Koenigsberger Ratio (Q)
And-Alb+Potassic+Calcic	2.85	0.19	0.52
Magnetite-Apatite*	3.80	1.84	1.09
Potassic (Bt)	2.78	0.13	0.36
Potassic (Kf)	3.02	0.52	0.83
Potassic+ Cal-Qtz-Py	3.10	0.41	0.70
Qtz-Cal-Chl-Py±Cpp±Hem	3.27	0.34	0.47
Sodic (Ab-Mt-Ti)	3.14	0.76	0.62
Sodic + Potassic (Bt)	2.98	0.52	3.31

Figure 21: Comparison of the petrophysical properties associated with different alteration types at Ernest Henry.

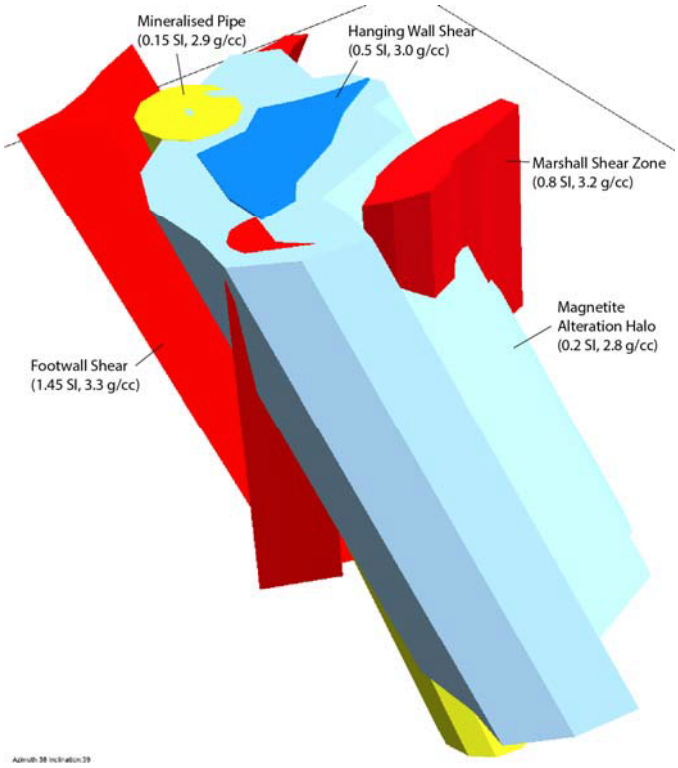

Figure 22: 3-D perspective of the Ernest Henry magnetic model generated in ModelVisionPro™. Susceptibility is indicated by the color of the bodies. The Marshall, and Footwall shears are the most magnetic the ore zone is the only weakly magnetic. The inverse magnetic zonation is due to oxidation in the mineralized zone. View is toward the NE.

Table 1: Comparison of key minerals for different alteration types at Ernest Henry.

Alteration type	Chalcopyrite	Chamosite	Pyrite	Albite	Microcline	Quartz
And-Alb+Potassic+Calcic	0.00	0.82	0.27	7.41	23.54	10.56
Magnetite-Apatite*	3.80	1.84	1.09	1.09	1.09	1.09
Potassic (Bt)	0.00	0.29	0.07	58.79	2.80	8.48
Potassic (Kf)	0.25	2.27	3.38	2.52	45.91	8.22
Potassic+ Cal-Qtz-Py	2.00	1.19	4.03	0.96	31.62	15.88
Qtz-Cal-Chl-Py±Cpp±Hem	2.88	10.26	13.96	0.16	2.70	33.56
Sodic (Ab-Mt-Ti)	0.00	0.31	0.31	54.96	3.73	2.38
Sodic + Potassic (Bt)	0.05	1.12	0.27	20.11	20.00	10.03

Canteen

At Canteen, mineralization is also mainly associated with late calcite-quartz-pyrite-dolomite-chlorite alteration assemblages (Table 2). However, the overprinting relationships are less consistent at Canteen than Ernest Henry, and copper is also associated with magnetite-apatite assemblages and Po-Calcite veining (e.g., Austin et al., 2016f). Mineralization associated with magnetite-apatite has high density and high magnetic susceptibility and NRM, but a relatively low Q, all due to the presence of coarse multi-domain magnetite. The pyrrhotite-breccias have high density, high NRM and Q, but only moderate susceptibility (e.g., 0.1 SI) which is comparable with most other lithologies at Canteen. Mineralization is mainly

present in fractures and veins, with pyrrhotite-calcite. The mineralized veins have low density and magnetic susceptibility values, but a moderate NRM and high Q, which is consistent with the presence of monoclinic pyrrhotite. By contrast, where mineralization is associated with the calcite-quartz-pyrite overprint, petrophysical values are low across the board, other than for elevated density where pyrite content is high. This is due to a number of factors, but mainly to the loss of magnetite and/or pyrrhotite, and precipitation of pyrite ± chlorite. The copper mineralization appears to be spatially associated with a number of faults that cross-cut the main NNW-trending magnetite-rich zone at Canteen (Fig 11), which causes zonation whereby a relatively reduced (e.g., magnetite-dominated) assemblage is overprinted by a more oxidized (e.g., pyrite-dominant) assemblage. This results in an inverse zonation between sulfur+copper (i.e., a proxy for copper sulfide) with susceptibility (i.e., a proxy for magnetite) at the deposit scale, as illustrated in Fig 23.

Therefore, at Canteen the petrophysical zonation is related to redox, insomuch as the earlier, more reduced assemblages have high magnetic susceptibility, related to their magnetite content. Conversely, the more oxidized, more mineralized assemblages which overprint the magnetite-rich zone are pyrite-rich, and whilst they have comparable density, they have significantly reduced magnetic susceptibility due to magnetite destruction coupled with pyrite precipitation.

Table 2: Comparison of petrophysical properties and associated mineral assemblages for various alteration types at Canteen. The numbers represent mean proportions of the mineral as a percentage of the total volume, based on estimates from TIMA analyses.

Alteration	Density	MagSus (SI)	NRM (A/m)	Koenigsberger	Albite	Andesine	Apatite	Biotite	Calcite	Chamosite	Clinochlore	Dolomite_Fe	Magnetite	Ilmenite	Pyrite	Pyrrhotite	Quartz	Titanite	Chalcopyrite
Biotite-Andesine ovp Sodic	2.9	0.11	14	7	3	23	0	19	2	0	1	0	2	0	0	0	6	1	0.0
Biotite-Andesine ovp Mt-Ap-Py	3.3	0.78	237	8	2	6	2	6	2	2	0	0	25	0	5	0	7	1	0.2
Ca-Py-Qtz-Mt	3.1	0.12	12	2	2	2	1	5	13	2	0	0	6	0	15	0	25	1	0.4
Ca-Po-Py-Qtz-Chl ovp Biot-And	2.9	0.12	26	7	19	14	0	17	10	1	0	5	1	0	1	1	10	0	0.0
Ca-Py-Qtz ovp Sodic	2.9	0.10	10	3	28	0	0	3	14	1	1	7	3	0	10	0	13	1	0.0
Cal-Py-Chl ovp Potassic ovp Sodic	2.8	0.15	16	3	24	1	0	10	8	0	6	0	4	0	2	0	5	2	0.7
Po-Calcite Bx	3.2	0.08	196	64	24	0	0	3	15	0	1	8	0	0	0	27	7	0	0.0
Po-Ca-Dol ovp Sodic	2.8	0.02	47	52	64	0	0	0	2	0	1	7	0	0	0	1	11	0	1.3
Potassic ovp Sodic	2.8	0.08	25	12	28	0	0	8	6	0	1	0	1	0	0	6	9	1	0.0

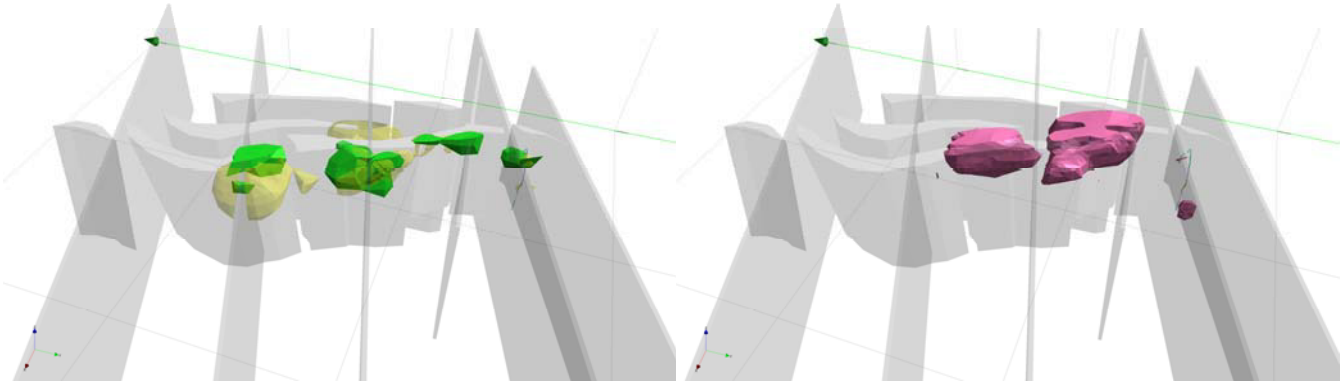

Figure 23: left. Interpolated volumes calculated for S (yellow) and Cu (green), using Leapfrog™ superimposed on the 3-D magnetic model generated using Modelvision™. Note the spatial coincidence of both Cu and S with the faults; right. Interpolated volumes calculated for magnetic susceptibility (pink) using Leapfrog™ superimposed on the 3-D magnetic model. Note the inverse spatial coincidence of susceptibility with the faults. In this case magnetic susceptibility is used as a proxy for magnetite content in the prospect. Model is viewed looking WSW, along the strike of the interpreted faults.

CONCLUSIONS

This is the first time any study has brought together so much petrophysical data from so many different styles of mineralization across a mineral district, and the results provide important constraints for future exploration for various styles of mineralization undercover. The deposits studied have a wide variety of petrophysical properties, primarily dictated by the relative contents of magnetic minerals (e.g., magnetite, monoclinic pyrrhotite, and hematite) and other non-magnetic minerals (e.g., hexagonal pyrrhotite, pyrite, galena, sphalerite, barite). Any combination of these minerals can be associated with high densities. High magnetic susceptibilities (and hence high amplitude magnetic anomalies) are invariably associated with coarse magnetite, whereas monoclinic pyrrhotite is associated with moderate magnetic susceptibility, high remanence (and potentially unusual magnetic anomalies). Hematite is only weakly magnetic.

Many deposits and prospects contain mixtures of different Fe-oxide and sulfide phases, which can be related to redox and/or overprinting.

1. Oxidized assemblages contain hematite, no pyrrhotite, but typically pyrite and variable magnetite. In IOCG systems hematite is associated with retrograde (magnetite-destructive) alteration, and Cu, Au and/or Mo- mineralization. In sedex systems hematite is formed distal to the source.
2. Intermediate assemblages are magnetite-rich, and often contain pyrrhotite and/or pyrite. In IOCGs systems they are often mineralized, but always associated with large positive magnetic anomalies, due to multidomain magnetite. In Sedex systems magnetite forms proximal to sources. Magnetite is advantageous for further mineralization, because it can be further oxidized or reduced.
3. Reduced assemblages are typically pyrrhotite dominant, contain no hematite, but often do contain magnetite. Hexagonal (non-magnetic) pyrrhotite is typically associated with galena and sphalerite in Sedex systems, whereas magnetic pyrrhotite is more typically associated with chalcopyrite in ISCGs.

The study has shown that where pyrrhotite is present it is usually subordinate to magnetite, and the magnetic field responses from the different components interfere (particularly at the resolution of the data) and cannot be easily separated. In cases where pyrrhotite is the dominant phase, it is commonly hexagonal (non-magnetic) pyrrhotite (e.g., Artemis, Maronan). Where monoclinic pyrrhotite is present the remanence is typically oriented sub-vertical up (e.g., Canteen, Cormorant, Maronan, Mt Colin), and as such, is difficult to isolate from the steep, upward north oriented inducing magnetic field.

REFERENCES

Austin, J.R. and Foss, C.A., 2014. Understanding iron oxide copper-gold (IOCG) magnetic targets from the inside out: case studies from northern Australia. Annual Geoscience Exploration Seminar (AGES), 18-19 March 2014, Alice Springs.

Austin, J.R., Gazley, M.F., Walshe, J.L., and Patterson, B.O., 2016b. Uncover Cloncurry – Summary: Integrated structural, metasomatic and metallogenic history of the Cloncurry District. CSIRO, Australia, EP166451, pp. 45.

Austin, J.R., Gazley, M.F., Walshe, J.L., Godel, B., leGras, M., and Paterson, B.O., 2016c. Uncover Cloncurry – The Monakoff Cu-Au-U deposit: Integrated Petrophysical and Geochemical analyses. CSIRO, Australia, EP165042, pp. 50.

Austin, J.R., Gazley, M.F., Godel, B., Hawkins, S., and leGras, M., 2016b. Uncover Cloncurry – The Maronan Pb-Ag deposit: Integrated Petrophysical and Geochemical analyses. CSIRO, Australia, EP165052, pp. 50.

Austin, J.R., Walshe, J.L., Gazley, M.F., Ibrahimi, T., Patterson, B.O., and leGras, M., 2016d. Uncover Cloncurry – The Ernest Henry Cu-Au deposit: Integrated Petrophysical and Geochemical analyses. CSIRO, Australia, EP165053, pp. 56.

Austin J.R., Gazley M.F., Ibrahimi T., Walshe J.L., and Patterson B.O., 2016e. Uncover Cloncurry – The E1 Cu-Au deposit: Integrated Petrophysical and geochemical analyses. CSIRO, Australia, EP165071, pp. 50.

Austin, J.R., Walshe, J.L., Gazley, M.F., Sisson, M., leGras, M., and Godel, B., 2016f. Uncover Cloncurry – The Canteen Cu-Au prospect: Integrated Petrophysical and geochemical analyses. CSIRO, Australia, EP165041, pp. 52.

Austin J.R., Gazley M.F., Patterson B.O., leGras M., and Walshe J.L., 2016g. Uncover Cloncurry – The Cormorant Cu-Au Prospect: Integrated Petrophysical and Geochemical analyses. CSIRO, Australia, pp. 44

Austin, J.R., Hawkins, S., Gazley, M.F., Patterson, B., leGras, M., Walshe. J.L., 2016h. The Mount Colin Au-Cu deposit: Integrated Petrophysical and geochemical analyses. CSIRO, Australia, pp. 32.

Gazley, M.F., Patterson, B.O., Austin, J.R., and Walshe, J.L., 2016b. Uncover Cloncurry – Osborne Cu-Au deposit: Integrated Petrophysical and Geochemical analyses. CSIRO, Australia, EP165511, pp. 25.

Gazley, M.F., Austin, J.R., Hawkins, S., Patterson, B.O., leGras, M., Godel, B., and Walshe, J.L., 2016c. The Kalman Mo-Re-Cu-Au deposit: Integrated Petrophysical and Geochemical analyses. CSIRO, Australia, EP165471, pp. 35.

Nystroem, J.O. and Henriquez, F., 1994. Magmatic features of iron ores of the Kiruna type in Chile and Sweden; ore textures and magnetite geochemistry. Economic Geology, 89(4), pp.820-839.

Patterson, B.O., Gazley, M.F., Austin, J.R., and Walshe, J.L., 2016. Uncover Cloncurry – The Merlin Mo-Re deposit: Integrated Petrophysical and Geochemical analyses. CSIRO, Australia, EP164990, pp. 30.